Phase-resolved pulsed precessional motion at a Schottky barrier

M. Buess,[1,2] T. P. J. Knowles,[1] U. Ramsperger,[1] D. Pescia,[1] and C. H. Back[2]
[1]*Laboratorium für Festkörperphysik, Eidgenössische Technische Hochschule Zürich, CH-8093 Zürich, Switzerland*
[2]*Institut für Experimentelle und Angewandte Physik, Universität Regensburg, Universitätsstrasse 31, 93040 Regensburg, Germany*
(Received 31 October 2003; revised manuscript received 2 March 2004; published 20 May 2004)

The precessional motion of the magnetization is excited by an ultrashort magnetic-field pulse at a Schottky barrier containing a ferromagnetic film. The precessional frequency, measured as a function of a bias field of variable strength and direction by time resolved Kerr microscopy, is accurately reproduced by a model based on the theory of ferromagnetic resonance. The spatially resolved precessional phase reveals a jump related to the chiral character of the exciting magnetic-field pulse.

DOI: 10.1103/PhysRevB.69.174422 PACS number(s): 75.30.Gw, 76.50.+g, 78.47.+p

At a metal-semiconductor interface forming a Schottky barrier one can apply a voltage and—provided free carriers are present in the barrier region—it may be possible to drive a current across the barrier. If the metallic side of the barrier is a ferromagnet, spin-polarized carriers can be injected from the ferromagnet into the semiconductor.[1,2] Spin injection from magnetic semiconductors acting as spin polarizers into nonmagnetic semiconductors has also been observed.[3] Vice versa, if spin-polarized carriers are excited in the semiconductor via optical orientation,[4] spin-polarized carriers may be ejected from the semiconductor into the ferromagnet. Such a current can affect the magnetic state of the ferromagnet it passes through, opening the possibility of controlling the magnetic state by applying a voltage.[5,6] We have recently reported on a similar device,[7] in which a focussed and short ($\approx$300 fs) pump laser was used to excite a current across a Schottky barrier consisting of an ultrathin FeCo film grown epitaxially onto GaAs. The magnetic-field pulse associated with the current launched the pulsed precessional motion (PPM) of the FeCo magnetization around its equilibrium position.

In this paper we present further experimental data that corroborate the ideas of Ref. 7. First, the precessional frequency is measured as a function of a static bias magnetic field with variable strength and direction, applied in the plane of the film. The obtained set of dispersion curves can be accurately modelled when the PPM is treated as small angle excitations of the magnetization vector within the framework of ferromagnetic resonance (FMR).[8] Second, noticing that the circulating vector field created by the current flowing perpendicular to the film plane establishes a chiral geometry, we set up to detect any sign of chirality in our experimental data.[7,9] Indeed, the spatially resolved precessional phase undergoes a jump at a line passing through the pump beam focus, as required by the chiral geometry.

In the present experiment, a *p*-doped GaAs crystal was cleaved under UHV conditions to obtain a clean and atomically flat GaAs(110) surface. Using molecular beam epitaxy, 3 monolayer (ML) of Au were deposited at 77 K followed by a 15 ML thick Fe film. The gold layer aims at preventing As interdiffusion into the Fe film which was reported to be correlated to a reduced magnetic moment.[10] The sample was capped with an additional passivating layer of 20 ML Au as all measurements were performed at ambient pressure. Film growth was monitored by scanning tunnelling microscopy and will be reported elsewhere. The static magnetic properties of the Fe film were characterized by magneto-optic Kerr effect measurements and by using a SQUID magnetometer (superconducting quantum interference device). Figure 1 shows hysteresis loops along the in-plane directions $\delta=0°$ ($[1\bar{1}0]$), $\delta=45°$ and $\delta=90°$ ($[001]$). These curves can be understood if the uniaxial anisotropy favoring the $[1\bar{1}0]$ in-plane direction is supplemented by an effective in-plane fourfold magnetic anisotropy.[11,12] As a consequence, the hysteresis curve along the easy $[1\bar{1}0]$ axis shows a square loop, while the one along $[001]$ has a slow linear increase at low magnetic fields, followed by a jump at a well defined ''split'' field H_s. Because of this behavior, the $[001]$ axis is referred to as the ''intermediate'' axis. This magnetization curve can be described by two parameters: The slope s of the initial section (or an extrapolation to the saturation magnetization, giving a saturation field $H_{sat}\approx 500$ Oe) and the value of $H_s\approx 164$ Oe. In addition, using SQUID magnetometry, we have measured the component of the magnetization perpendicular to the easy plane as it rotates out of the plane and determined that an effective field of about $4\pi M_{eff}=4\pi M_0 - 2K_\perp/M_0$ is required to reach saturation along the normal. Here, $K_\perp$ is a uniaxial perpendicular anisotropy caused by the two Fe/Au interfaces. This kind of anisotropy is not uncommon for ultrathin ferromagnetic layers.[13,14] Important for the experiments reported below is the effective field required to pull the magnetization out of the plane of the film. It is of the order of 16 ± 2 kOe, see inset Fig. 1. From s, H_s, and $4\pi M_{eff}$ one can reconstruct the various magnetic constants appearing in the magnetic energy density.[12] We will see that magnetic spectroscopy—i.e., the determination of the frequency of the precessional motion as a function of the applied magnetic-field vector—allows to refine the findings from static magnetization measurements.

The time evolution of the magnetization $\vec{M}$ was measured in a pump-probe experiment. $\vec{M}$ is tipped away from its equilibrium position by subjecting it to a fast rise time magnetic-field pulse H_p perpendicular to the magnetization direction, but in the film plane. To apply the pump pulse, we use the scheme of internal field generation in a Schottky diode.[7] The metal-semiconductor interface is used as the source of the magnetic pulse itself. A focussed 300 fs laser pulse from a

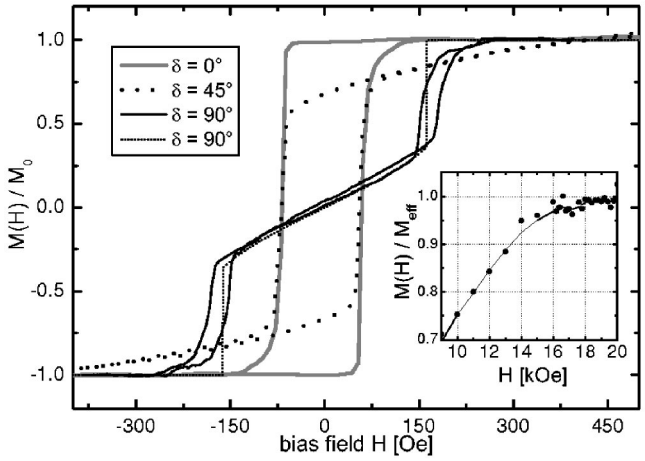

FIG. 1. Kerr effect hysteresis loops measured along the in-plane directions $\delta=0°$ (easy axis), $\delta=45°$, and $\delta=90°$ (intermediate axis). The dotted line shows the calculated curve for $\delta=90°$ using the parameters K_u, K_1, and K_2 obtained from the fit shown in Fig. 3.

Ti:Sappire oscillator (4.75 MHz repetition rate, 800 nm, energy per pulse ≈ 1.5 mJ/cm^{-2}, focus 1 μm) generates a photocurrent, which in turn gives rise to a fast rise time magnetic-field pulse. The probe pulse (400 nm wavelength, energy per pulse ≈ 0.75 mJ/cm^{-2}, 0.5 μm focus), placed at a variable position with respect to the pump beam, is used to probe the perpendicular component of $\vec{M}$ using the polar magneto-optical Kerr effect. The probe pulse is delayed by a time τ with respect to the pump pulse using an optical delay line. A detailed description of the experimental method is found in Ref. 7. In addition to H_p, a static magnetic bias field H with variable strength is applied along various directions in the plane of the film. A typical trace of $M_z(t)$ is shown for $H=0$ in Fig. 2. $M_z(t)$ oscillates as expected from a precessional motion. For all $\vec{H}$ similar curves were measured, from which a well defined frequency could be obtained by fast Fourier transform (FFT) as shown in the inset of Fig. 2. Zero-filling and a Hamming cutoff window is used

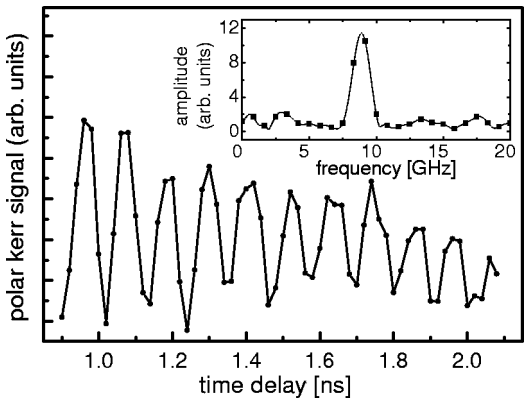

FIG. 2. Typical time domain data ($H=0$). The inset shows the FFT of the time domain data. The dots represent the FFT from the raw data, while zero padding was used for the continuous line. The peak position f gives a data point in Fig. 3.

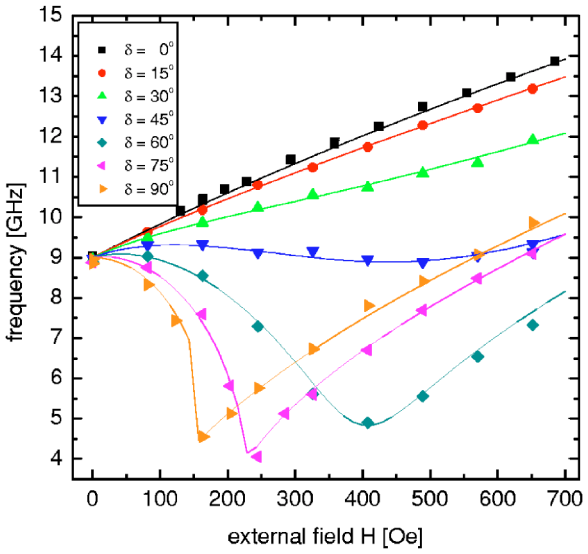

FIG. 3. Bias field dependence of precessional frequency f. Displayed are the dispersion curves for different bias field angles δ as measured (dots) and calculated (curves). The curve changes gradually from the monotonic field dependence for the easy axis $\delta=0°$ to a more complex behavior for the intermediate axis $\delta=90°$.

to extract the frequency from the time scans with finite (1.2 ns) length.

Figure 3 shows the precessional frequency f vs bias field strength H for different angles δ between the field direction and the easy magnetization direction in the plane of the film. For $\delta=0°$ the frequency f increases monotonically with the bias field H. This is the behavior expected for a field applied along the easy magnetization direction and has been reported previously. The data for $\delta=90°$ shows a more complex behavior. At low H, f decreases, until a minimum at $H_s=162$ Oe is reached, followed by an increase of f. This decrease of the precessional frequency is known from FMR experiments[8,14] along an intermediate axis of the type described above. Typically, it occurs because a magnetic field applied along the intermediate axis pulls the global minimum of the energy landscape—which determines the equilibrium direction of the magnetization vector—closer to the intermediate axis, making it more shallow in the process. As the precessional frequency is essentially determined by the curvature of the energy landscape at the minimum, the precessional mode is softened. At other angles, the monotonous increase of f and its tendency of undergoing a minimum are both present with different weights: the actual behavior depends upon which effect is more relevant. Notice that $H_p \leqslant 25$ Oe is small with respect to the various fields present in the film and it is terminated after some 100 ps, so that it can be neglected when calculating the precessional frequency. As the deviation from equilibrium produced by such a small H_p is very small and the exchange length is much smaller than the spatial extent of the pulse, we will neglect exchange fields as well.

The solution for reproducing the set of curves in Fig. 3 comes from a very simple thought. For small deviations from equilibrium, the Landau-Lifshitz equation for the spin mo-

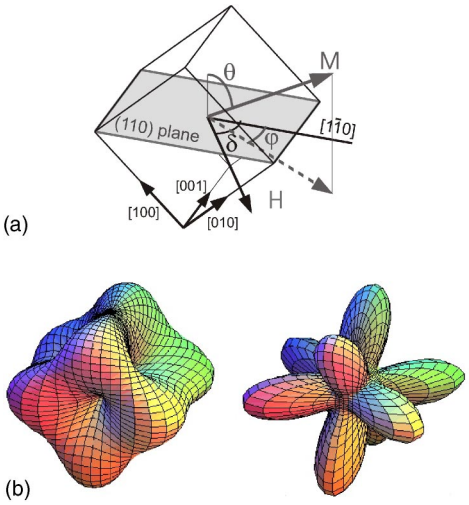

FIG. 4. (a) Crystallographic coordinates and definition of angles. The cube illustrates the orientation of the crystallographic unit cell of bcc iron. The magnetization direction is expressed by the spherical coordinates $(\varphi,\ \theta)$. The external magnetic field vector H lies in the (110) plane of the film defined by the angle δ to the easy axis $[1\bar{1}0]$. (b) Illustration of energy surfaces of the first two anisotropy terms with cubic symmetry used in Eq. (2).

tion reduces to the equation of a classical harmonic oscillator. The PPM experiment corresponds to establishing an initial condition slightly off equilibrium for the magnetization vector and letting the motion evolve accordingly. The ''harmonic oscillator'' will oscillate according to its eigenfrequency, the very same frequency which must be used to drive a forced harmonic oscillator at resonance. Thus, we expect the precessional frequency being given by a well-known general expression for the FMR frequency written in term of the magnetic energy density $\mathcal{E}(\theta,\varphi)$ where the magnetization vector is expressed in spherical coordinates θ and φ:[16]

$$2\pi f=\frac{\gamma}{M_0\sin\theta}\sqrt{\frac{\partial^2\mathcal{E}}{\partial\varphi^2}\frac{\partial^2\mathcal{E}}{\partial\theta^2}-\frac{\partial^2\mathcal{E}}{\partial\varphi\partial\theta}}\Bigg|_{\theta=\theta_0,\varphi=\varphi_0}, \quad (1)$$

where $\mathcal{E}(\theta,\varphi)$ is the magnetic energy density, θ measures the angle of $\vec{M}$ with respect to the normal to the film, φ is the angle formed by $\vec{M}$ and the easy in-plane magnetization axis, θ_0,φ_0 give the equilibrium position of $\vec{M}$, M_0 represents the saturation magnetization, and $\gamma=g/2(e/m_ec)$ is the gyromagnetic ratio. The coordinate system is shown in Fig. 4(a). This expression relates the precessional frequency to the curvature of the energy landscape at its minimum. Thus, the key to applying this expression is to formulate a model of $\mathcal{E}(\theta,\varphi)$ that captures the essential magnetic interactions in our system. Guided by previous investigations of similar systems[11,12] we write $\mathcal{E}(\theta,\varphi)$ as the sum of five terms:

$$\begin{aligned}\mathcal{E}(\varphi,\theta)=&-|H|M_0\cos(\varphi-\delta)\sin(\theta)+2\pi M_{eff}M_0\cos^2\theta\\&+K_1(\alpha_1^2\alpha_2^2+\alpha_2^2\alpha_3^2+\alpha_3^2\alpha_1^2)+K_2(\alpha_1^2\alpha_2^2\alpha_3^2)\\&+K_u\sin^2\varphi. \quad (2)\end{aligned}$$

The first contribution to $\mathcal{E}(\varphi,\theta)$ is the Zeeman energy, which contains the angle δ between $\vec{H}$ and the easy axis $[1\bar{1}0]$. Both $|H|$ and δ are varied in the experiment. The second term is the energy arising mainly from the dipolar interaction favoring the in-plane magnetization. This effective term consists of the dipolar contribution and an additional perpendicular anisotropy energy originating from the Fe/Au interfaces which opposes the dipolar term and thus reduces the effective field required to pull the magnetization out of the plane.[13,14] The next two terms with coupling constants K_1 and K_2 describe the bcc Fe magnetocrystalline anisotropies exhibiting the symmetry of the lattice. K_1 is a standard cubic anisotropy containing the fourth power of the magnetization, and is necessary to obtain the shifted hysteresis curve of Fig. 1.[11] K_2 is a higher-order magnetic anisotropy absent in the analysis of similar systems[11,12,14] and introduced here to correct for deviations of the fit from the experimental set of curves.[15] Notice that the direction cosines α_i refer to the cubic axis of the lattice: they can be expressed in terms of the coordinate system proper to our 110 surface by the following transformation, see Fig. 4(b):

$$\begin{pmatrix}\alpha_1\\ \alpha_2\\ \alpha_3\end{pmatrix}=\begin{pmatrix}1 & & \\ & \frac{1}{\sqrt{2}} & -\frac{1}{\sqrt{2}}\\ & \frac{1}{\sqrt{2}} & \frac{1}{\sqrt{2}}\end{pmatrix}\begin{pmatrix}\sin(\theta)\cos(\varphi)\\ \sin(\theta)\sin(\varphi)\\ \cos(\theta)\end{pmatrix}. \quad (3)$$

The term $K_u\sin^2\varphi$ is an in-plane uniaxial anisotropy favoring $[1\bar{1}0]$ as easy magnetization direction. This term is required to explain the large in-plane uniaxial anisotropy often observed in these systems.[11,12,14] Its origin most likely lies in strain introduced by the lattice mismatch between substrate and thin film. Even in very thick bulk bcc Fe films, where terms originating from the interface should be negligible, this additional term is still present.[17]

As the value M_0 cancels out in Eq. (1), the parameters at our disposal for fitting the dispersion curves containing $N=75$ data points are the anisotropy constants K_u, K_1, and K_2. We also let the $4\pi M_{eff}$ vary during the fit, with the aim of obtaining a fitted value around 16 ± 2 kOe, which is consistent with our SQUID data. Notice that the g factor and $4\pi M_{eff}$ essentially determine the overall frequency level of the dispersion curves. Therefore these two parameters are strongly coupled and one of them must be fixed to avoid an additional degree of freedom in the system. We choose to fix the g factor at 2.09, the value for bulk Fe. In contrast, the angular dependence of the dispersion curves is determined by the anisotropies K_u, K_1, and K_2. The fit includes numerically calculating for each value of $|H|$ and δ the equilibrium angle φ_0 of the magnetization vector from the equation $\partial\mathcal{E}/\partial\varphi=0$ and evaluating Eq. (1) at $(\varphi_0,\theta_0=\pi/2)$. In each step the sum of squared deviations $\Delta=\Sigma_i(f_i^{obs}-f_i^{calc})^2$ was optimized as a single function of all data points and the parameters K_u, K_1, K_2, and $4\pi M_{eff}$. The result of using Eq. (1) to fit the experimental dispersion curves are the continuous curves in Fig. 3. The mean deviation between the

experimental data and the continuous curves $\sqrt{\Delta/N-1}$ amount to 0.11 GHz, i.e., it is well below the width of the peaks obtained by the Fourier transformation of the time domain data. The values for the parameters we obtain by the fits are $K_1/M_0=194.3$ Oe, $K_2/M_0=-128.8$ Oe, $K_u/M_0=75.0$ Oe, $4\pi M_{eff}=17195$ Oe. The statistical error of the anisotropy constants resulting from starting the fit with a different set of initial values is less than 0.3 Oe and justifies that parameter sets very close to the global minimum are reached. The inclusion of K_2 into the model is necessary to correctly reproduce the angular dependence of the oscillation frequency f.[15] The dotted curve in Fig. 1(a) is the magnetization curve along the intermediate axis calculated from the parameters obtained from Fig. 3. The excellent modeling of the experimental data of Figs. 1 and 3 shows that PPM is indeed realized at a Schottky barrier and that standard methods developed for FMR can be applied to PPM as well.

We now consider the chiral aspect of PPM in this geometry. Responsible for launching the PPM is, according to the Landau-Lifshitz equation, the initial torque $\vec{H}_p \times \vec{M}$. A current flowing across the barrier (i.e., along the z axis) produces a magnetic vector field H_p circulating in the plane of the film (the x-y plane): this establishes a chiral geometry. Its center (which we take as the origin of the coordinate system) coincides with the focus of the pump beam. Let us take the x axis along the equilibrium $\vec{M}$ and no bias field applied. The chirality of H_p defines two half planes meeting at the line $x=0$. Let us assume that in the half plane $x>0$ the initial torque that triggers the motion points along z and will tip $\vec{M}$ below the film plane. In the half plane $x<0$ the torque points along $-z$ and $\vec{M}$ will be tipped above the film plane. The amplitude of the corresponding oscillation of the $M_z(\tau)$ component is achiral, as shown in the pattern published in Ref. 9, and thus is symmetric with respect to the line $x=0$, see also Fig. 5(a). The phase of the oscillation, instead, should change abruptly when going from $x<0$ to $x>0$ [Fig. 5(b)]. The spatially resolved maps of the amplitude of the oscillation [Fig. 5(c)] and its phase [Fig. 5(d)] follow closely the theoretically calculated patterns (Figs. 5(a) and 5(b), respectively). The maps Figs. 5(c) and 5(d) have been determined by plotting the maximum amplitude and the phase obtained in the FFT of the data as a function of the position of the probe beam. A 180° phase shift in the oscillations can be directly read out from the phase of the FFT at the resonance frequency. While an achiral pattern similar to Fig. 5(c) has already been observed in this geometry,[9] the phase shift between the two half planes reported in Fig. 5(d) is measured here, to our knowledge, for the first time. We point out that this chiral experimental geometry may be useful for experiments in which spin-polarized carriers are ejected into the metal film with their spin polarization along the normal of the film. In this case, the situation is achiral. Thus, measuring the phase will be an unambiguous test of torque transfer from the spin polarization of the carriers to the magnetization of the film.[5]

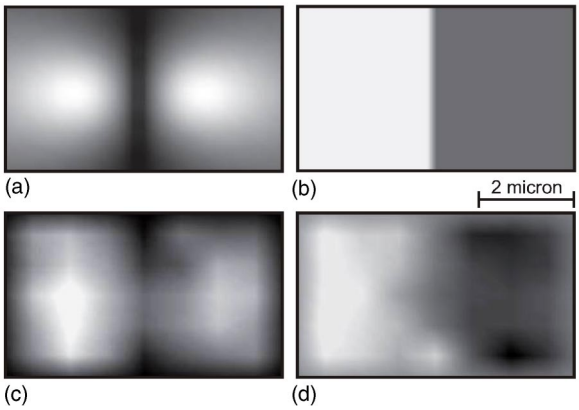

FIG. 5. (a) Two-dimensional maps of the torque amplitude in zero bias field. (b) Map of the torque sign (white = positive, black = negative). (c) Measured spatially resolved oscillation amplitude as a function of the position of the probe beam with respect to the pump beam (center). (d) Measured spatially resolved phase-shift of the oscillation as a function of the position of the probe beam with respect to the pump beam (center).

In summary, we have shown that it is possible to derive the static anisotropy constants with high accuracy using a PPM experiment in the time domain. The experiment can be used in a similar way as standard FMR measurements. However, notice that PPM can probe a much smaller quantity of spins than a standard FMR measurement: in this particular experiment we sample the response of 10^9 spins. A next step in future experiments will be to use the chiral aspect of PPM to answer interesting questions in the exciting field of spin manipulation in ferromagnet-semiconductor heterostructures. In particular, it should be possible to address the question of ejection of spin-polarized carriers from a semiconductor into a ferromagnetic metal.

We are thankful for stimulating discussions with G. Bayreuther. Financial support from Swiss National Foundation is gratefully acknowledged.

[1] H.J. Zhu, M. Ramsteiner, H. Kostial, M. Wassermeier, H.P. Schonherr, and K.H. Ploog, Phys. Rev. Lett. **87**, 016601 (2001).
[2] A.T. Hanbicki, B.T. Jonker, G. Itskos, G. Kioseoglou, and A. Petrou, Appl. Phys. Lett. **80**, 1240 (2002).
[3] R. Fiederling, M. Keim, G. Reuscher, W. Ossau, G. Schmidt, A. Waag, and L.W. Molenkamp, Nature (London) **402**, 787 (1999); Y. Ohno, D.K. Young, B. Beschoten, F. Matsukura, H. Ohno, and D.D. Awschalom, *ibid.* **402**, 790 (1999).
[4] D.T. Pierce and F. Meier, Phys. Rev. B **13**, 5484 (1976).
[5] S.I. Kiselev, J.C. Sankey, I.N. Krivorotov, N.C. Emley, R.J. Schoelkopf, R.A. Buhrman, and D.C. Ralph, Nature (London) **425**, 380 (2003) and references therein.
[6] A. Ney, C. Pampuch, R. Koch, and K.H. Ploog, Nature (London) **425**, 485 (2003) and references therein.

[7] Y. Acremann, M. Buess, C.H. Back, G. Bayreuther, and D. Pescia, Nature (London) **414**, 51 (2001).
[8] D.M. Engebretson, J. Berezovsky, J.P. Park, L.C. Chen, C.J. Palmstrom, and P.A. Crowell, J. Appl. Phys. **91**, 8040 (2002).
[9] C.H. Back, R. Allenspach, W. Weber, S.S.P. Parkin, D. Weller, E.L. Garwin, and H.C. Siegmann, Science **285**, 864 (1999).
[10] J.J. Krebs, B.T. Jonker, and G.A. Prinz, J. Appl. Phys. **61**, 2596 (1987).
[11] R. Höllinger, M. Zölfl, R. Moosbühler, and G. Bayreuther, J. Appl. Phys. **89**, 7136 (2001).
[12] M. Dumm, M. Zölfl, R. Moosbühler, M. Brockmann, T. Schmidt, and G. Bayreuther, J. Appl. Phys. **87**, 5457 (2000).
[13] Z. Celinski and B. Heinrich, J. Appl. Phys. **70**, 5935 (1991).
[14] G.A. Prinz, G.T. Rado, and J.J. Krebs, J. Appl. Phys. **53**, 2087 (1982).
[15] Without the K_2 term, the fit fails at $\delta = 0°$ and $\delta = 90°$, and Δ is increased by one order of magnitude. In the literature there exists no clear picture about the origin, the size and even the sign of this anisotropy constant. We note here, that our special system of Au/Fe/Au/GaAs(100) must not be compared to bulk bcc Fe. A more thorough investigation of this term as a function of temperature and thickness is beyond the scope of this paper.
[16] A.H. Morrish, *The Physical Principles of Magnetism* (Wiley, New York, 1965), pp. 551–553.
[17] G. Bayreuther (private communication).